Temperature Estimation in Permanent Magnet Synchronous Motors

ERICK AXEL MARTINEZ RIOS

Introduction

Permanent Magnet Synchronous Motors (PMSMs) [1,2,3]:

•High power and torque density.

•Widely used in electric powertrains, wind power generation, and robotics.

Potential Faults [4,5]:

Electrical, mechanical, and magnetic faults can occur.

Faults are caused by stresses during prolonged operation and varying power source/load parameters.

Introduction

Magnetic and Electric Faults [4,5]:

Heat generation in the motor can increase temperature, leading to potential **demagnetization** of permanent magnets or **melting insulation** in windings.

Demagnetization reduces the machine's torque capability and melting insulation can produce short circuits.

Temperature Monitoring [4,5]:

Essential for controlling PMSMs effectively and preventing thermal overloading.

Literature Review

- PMSM Temperature Estimation Methods [6,7]
  - Sensors
    - Required structural modifications and high cost.
  - Finite Element Analysis and Computational Fluid Analysis
    - Time-consuming and computationally complex.
    - Not real-time feasibility.
  - Thermal and Electrical Models
    - Challenging parameter estimation.

Data-driven methods

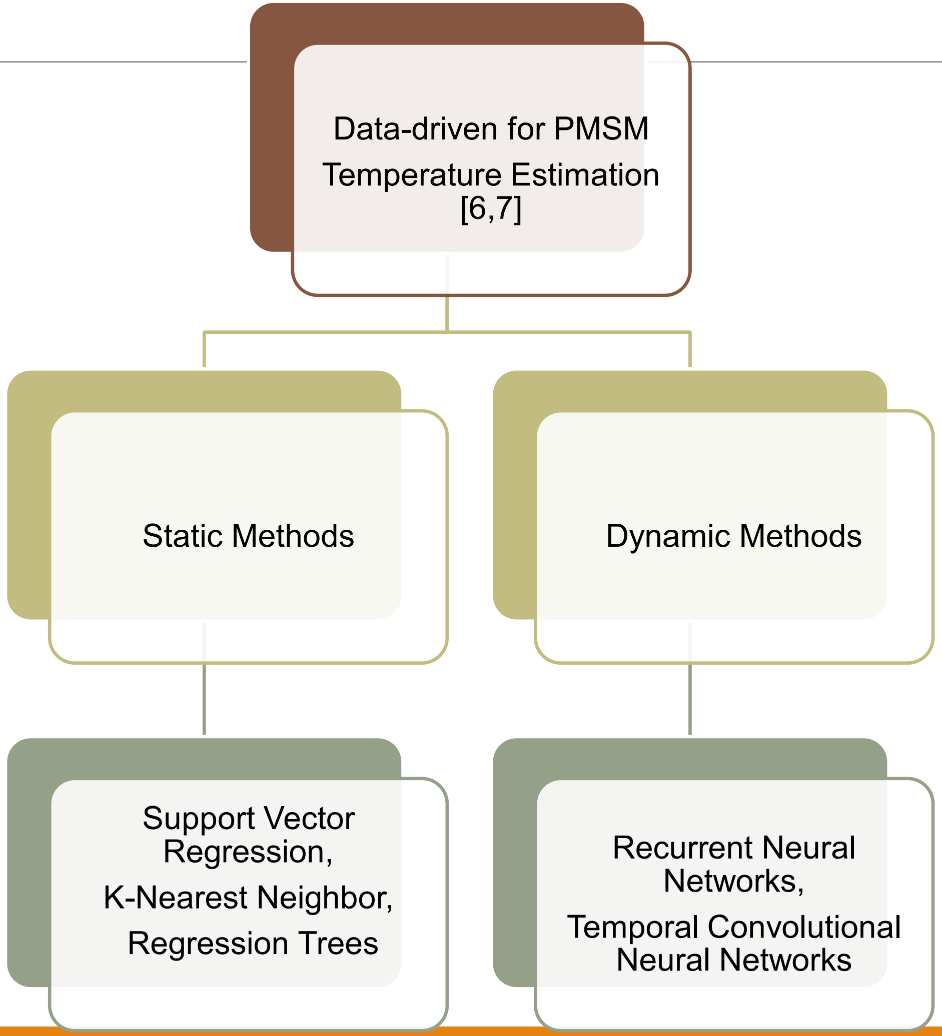

Data-driven methods drawbacks:

- Lack of interpretability (black-box methods).
- Machine learning requires large sample sizes and training times.
- Gathering sufficient quality data could be time-consuming and unrealistic.

Hammerstein Model

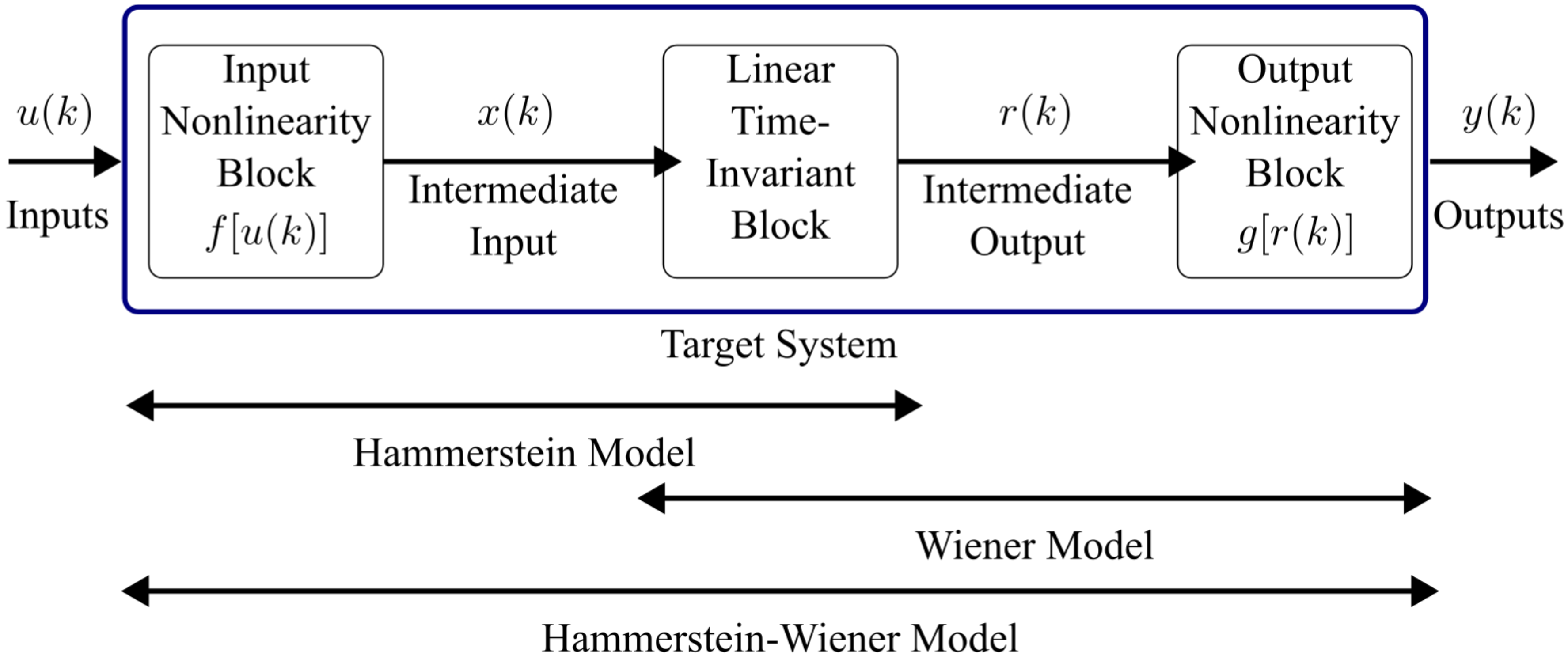

Figure 1. General structure of a Hammerstein-Wiener model [8].

NLARX model structure

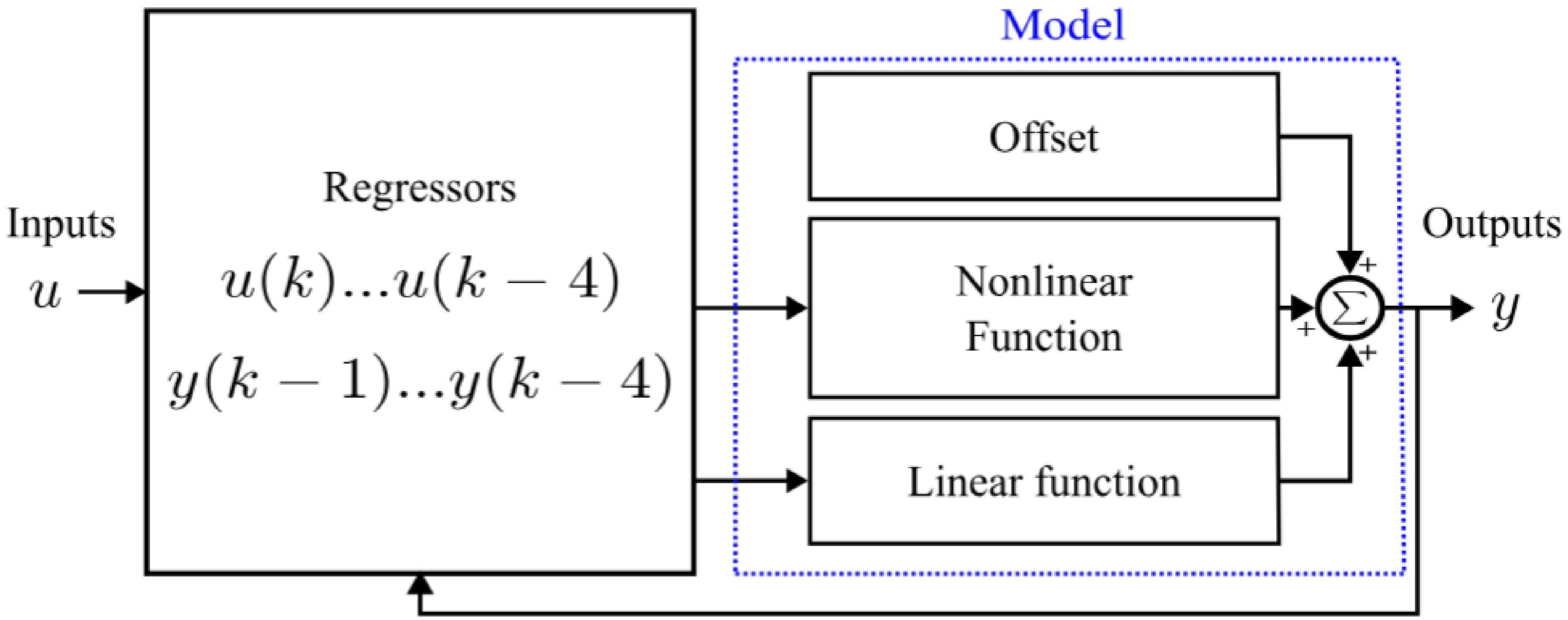

Figure 2. NLARX model structure.

Modified LPTN

The LPTN used in this work is based on the one proposed by Wallschied et al. [6]

The LPTN consists of varying resistances depending on speed and temperature.

The varying thermal resistances were changed by a fixed thermal resistance in series with a varying temperature source.

θ: Temperature
R, a: Thermal Resistance
P: Power Loss

y: Stator Yoke
w: Stator Winding
t: Stator Tooth
m: Permanent Magnet
θ_c: Coolant Temperature
θ_a: Ambient Temperature

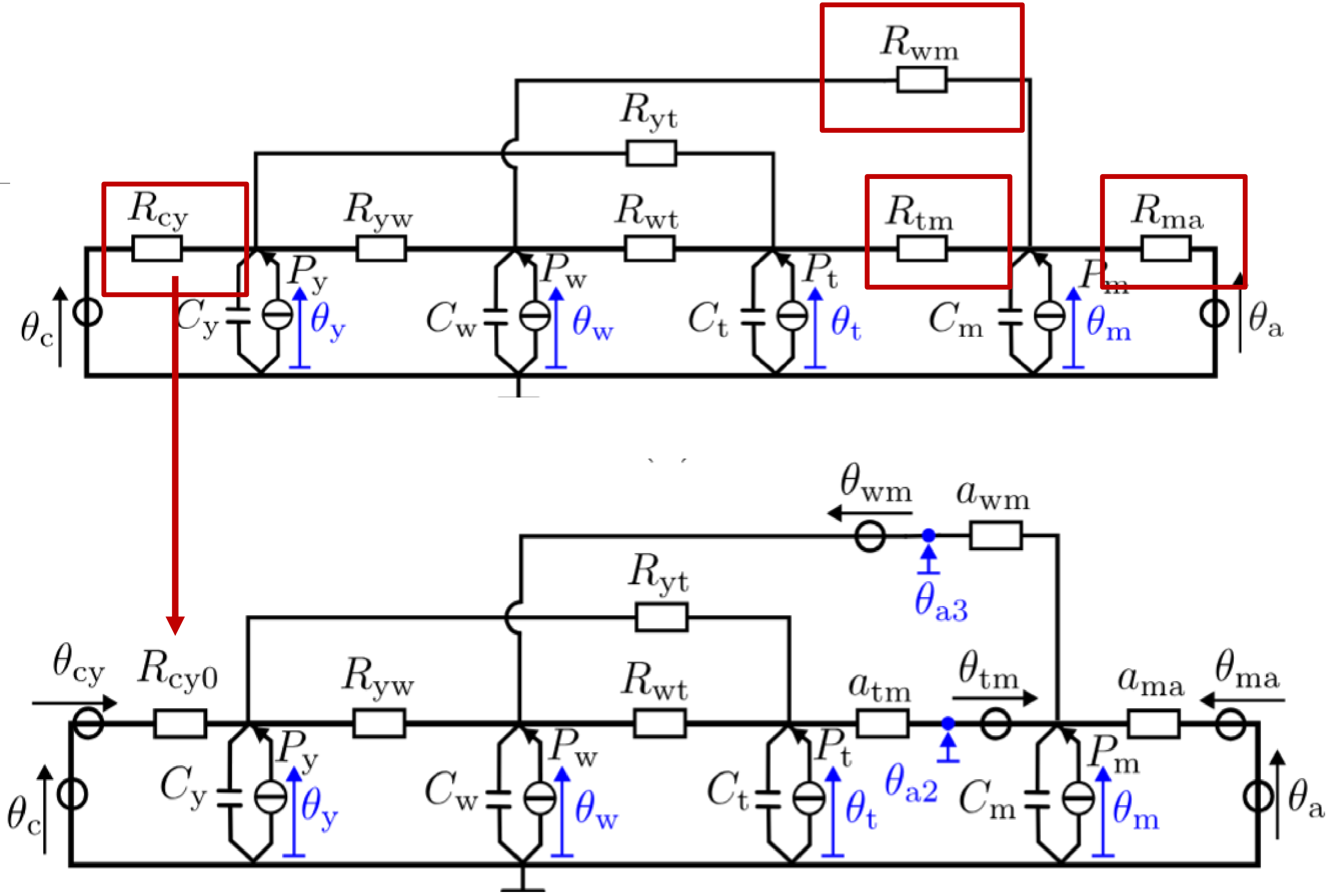

Figure 3. Modified lumped parameter thermal network of the PMSM.

$$\dot{\mathbf{x}} = \mathbf{A}\mathbf{x} + \mathbf{B}\mathbf{u},$$
$$\mathbf{y} = \mathbf{C}\mathbf{x} + \mathbf{D}\mathbf{u}$$

$$\mathbf{A} = \begin{bmatrix} \frac{1}{C_\mathrm{y}} & 0 & 0 & 0 \\ 0 & \frac{1}{C_\mathrm{w}} & 0 & 0 \\ 0 & 0 & \frac{1}{C_\mathrm{t}} & 0 \\ 0 & 0 & 0 & \frac{1}{C_\mathrm{m}} \end{bmatrix} \begin{bmatrix} -(G_\mathrm{yw} + G_\mathrm{yt} + G_\mathrm{cy0}) & G_\mathrm{yw} & G_\mathrm{yt} & 0 \\ G_\mathrm{yw} & -(G_\mathrm{yw} + G_\mathrm{wt}) & G_\mathrm{wt} & \frac{1}{a_\mathrm{wm}} \\ G_\mathrm{yt} & G_\mathrm{wt} & -\left(G_\mathrm{yt} + G_\mathrm{wt} + \frac{1}{a_\mathrm{tm}}\right) & 0 \\ 0 & 0 & \frac{1}{a_\mathrm{tm}} & -\left(\frac{1}{a_\mathrm{wm}} + \frac{1}{a_\mathrm{ma}}\right) \end{bmatrix}$$

$$\mathbf{B} = \begin{bmatrix} \frac{1}{C_\mathrm{y}} & 0 & 0 & 0 \\ 0 & \frac{1}{C_\mathrm{w}} & 0 & 0 \\ 0 & 0 & \frac{1}{C_\mathrm{t}} & 0 \\ 0 & 0 & 0 & \frac{1}{C_\mathrm{m}} \end{bmatrix} \begin{bmatrix} 1 & 0 & 0 & 0 & \frac{1}{R_\mathrm{cy0}} & 0 & 0 & 0 \\ 0 & 1 & 0 & 0 & 0 & 0 & 0 & -\frac{1}{a_\mathrm{wm}} \\ 0 & 0 & 1 & 0 & 0 & 0 & \frac{1}{a_\mathrm{tm}} & 0 \\ 0 & 0 & 0 & 1 & 0 & \frac{1}{a_\mathrm{ma}} & -\frac{1}{a_\mathrm{tm}} & \frac{1}{a_\mathrm{wm}} \end{bmatrix}, \quad \mathbf{C} = \mathbf{I}_{4\times 4}, \quad \mathbf{D} = \mathbf{0}_{4\times 8},$$

$$\mathbf{x} = \begin{bmatrix} \theta_\mathrm{y} & \theta_\mathrm{w} & \theta_\mathrm{t} & \theta_\mathrm{m} \end{bmatrix}^\top, \quad \mathbf{u} = \begin{bmatrix} P_\mathrm{y} & P_\mathrm{w} & P_\mathrm{t} & P_\mathrm{m} & \theta_\mathrm{cv} & \theta_\mathrm{av} & \theta_\mathrm{a2} & \theta_\mathrm{a3} \end{bmatrix}^\top.$$

Auxiliary Temperatures

$$\theta_{\mathrm{a2}} = \left(\theta_{\mathrm{m}} + \boxed{R_{\mathrm{tm1}}} a_{\mathrm{tm}}^{-1}\theta_{\mathrm{t}}\right)\left(1 + R_{\mathrm{tm1}} a_{\mathrm{tm}}^{-1}\right)^{-1},$$

$$\theta_{\mathrm{a3}} = \left(\theta_{\mathrm{w}} + \boxed{R_{\mathrm{wm1}}} a_{\mathrm{wm}}^{-1}\theta_{\mathrm{m}}\right)\left(1 + R_{\mathrm{wm1}} a_{\mathrm{wm}}^{-1}\right)^{-1}$$

Varying Temperatures Sources

$$\theta_{\mathrm{wm}} = \boxed{R_{\mathrm{wm1}}} a_{\mathrm{wm}}^{-1}\left(1 + R_{\mathrm{wm1}} a_{\mathrm{wm}}^{-1}\right)^{-1}\left(\theta_{\mathrm{w}} - \theta_{\mathrm{m}}\right),$$

$$\theta_{\mathrm{tm}} = \boxed{R_{\mathrm{tm1}}} a_{\mathrm{tm}}^{-1}\left(1 + R_{\mathrm{tm1}} a_{\mathrm{tm}}^{-1}\right)^{-1}\left(\theta_{\mathrm{m}} - \theta_{\mathrm{t}}\right),$$

$$\theta_{\mathrm{ma}} = \boxed{R_{\mathrm{ma1}}} a_{\mathrm{ma}}^{-1}\left(1 + R_{\mathrm{ma1}} a_{\mathrm{ma}}^{-1}\right)^{-1}\left(\theta_{\mathrm{m}} - \theta_{\mathrm{a}}\right),$$

$$\theta_{\mathrm{cy}} = \boxed{R_{\mathrm{cy01}}} R_{\mathrm{csy0}}^{-1}\left(1 + R_{\mathrm{cy01}} R_{\mathrm{csy0}}^{-1}\right)^{-1}\left(\theta_{\mathrm{y}} - \theta_{\mathrm{c}}\right).$$

Final coolant and ambient temperature sources

$$\theta_{\mathrm{cv}} = \theta_{\mathrm{c}} + \theta_{\mathrm{cy}},$$

$$\theta_{\mathrm{av}} = \theta_{\mathrm{a}} + \theta_{\mathrm{ma}}.$$

3-Fold Cross-Validation

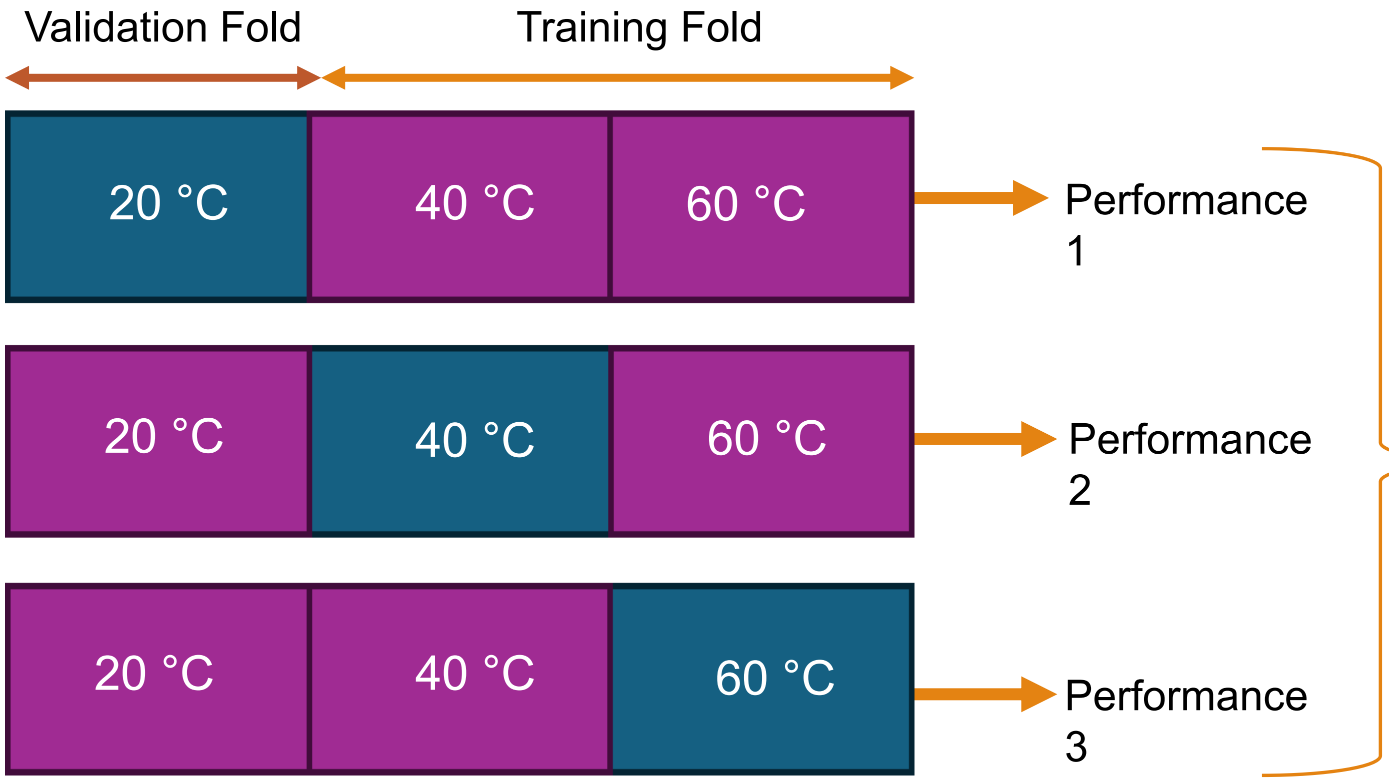

$$\sum_{i=1}^{3} \frac{Performance_i}{3}$$

$$MSE = \frac{1}{n}\sum_{i=1}^{n}(y_i - \hat{y}_i)^2$$

$$RMSE = \sqrt{\frac{1}{n}\sum_{i=1}^{n}(y_i - \hat{y}_i)^2}$$

$$MAE = \frac{1}{n}\sum_{i=1}^{n}|y_i - \hat{y}_i|$$

$$NRMSE = \frac{RMSE}{\sigma_y}$$

where n is the number of observations or data points, y_i is the actual observation of the i-th observation, and $\hat{y}_i$ is the predicted value of the i-th observation.

Dataset

- The dataset was obtained from a 200kW radial-flux PMSM with surface-mounted permanent magnets in the outer rotor and distributed winding for traction applications.

- The driving cycle was repeated for three inlet temperatures: 20 °C, 40 °C, and 60 °C.

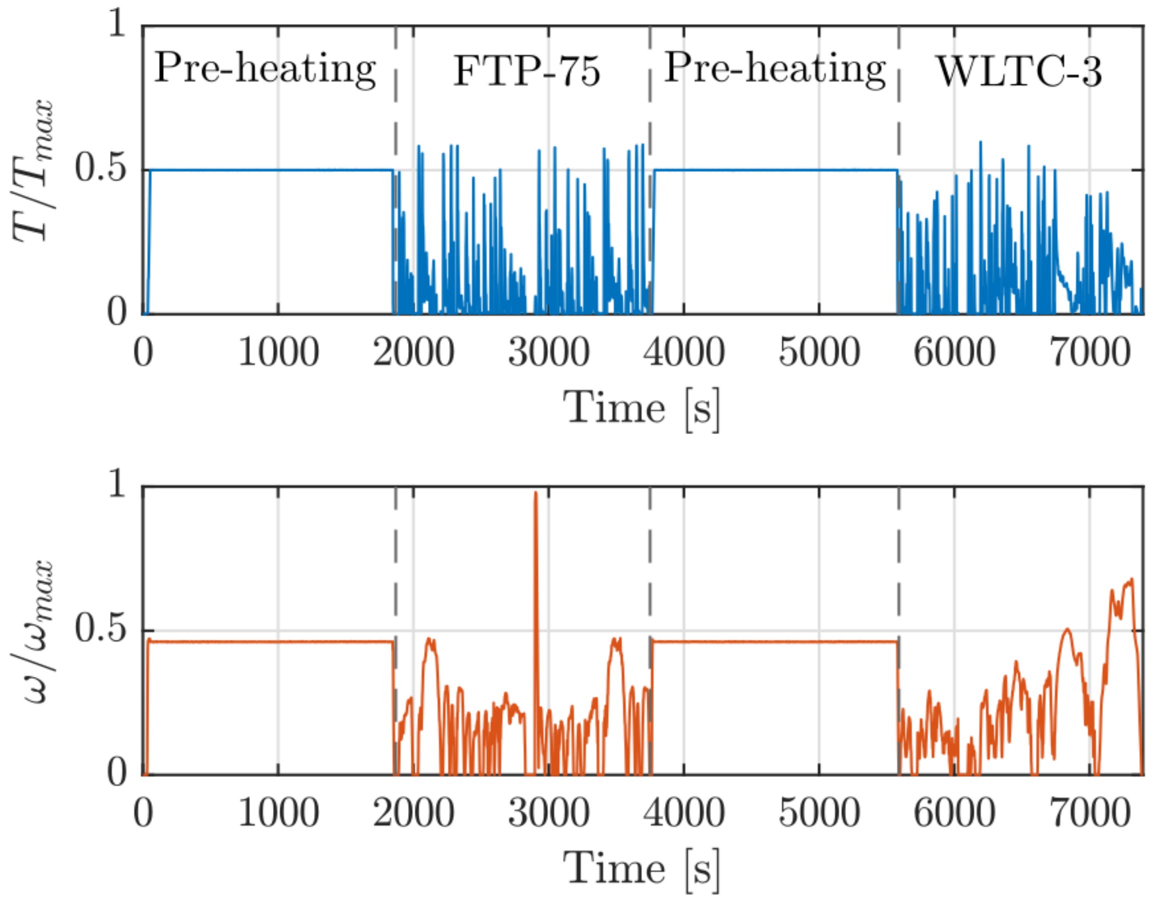

Figure 4. Normalized torque and speed of the PMSM in the driving cycle.

In-wheel motor back-to-back test setup.

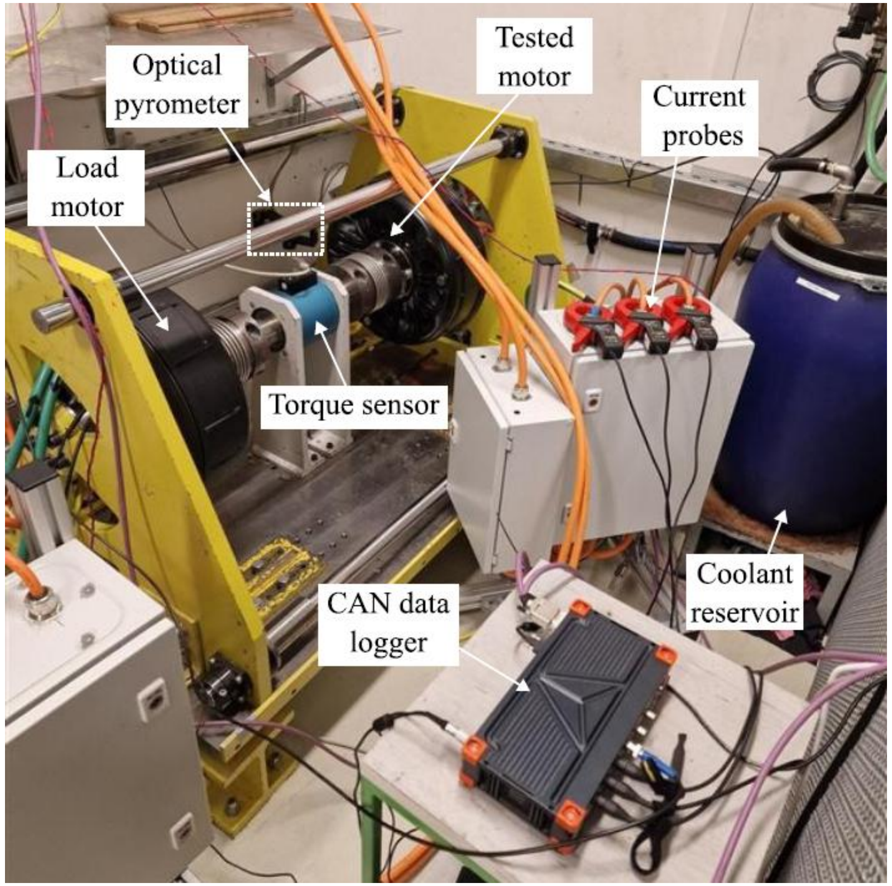

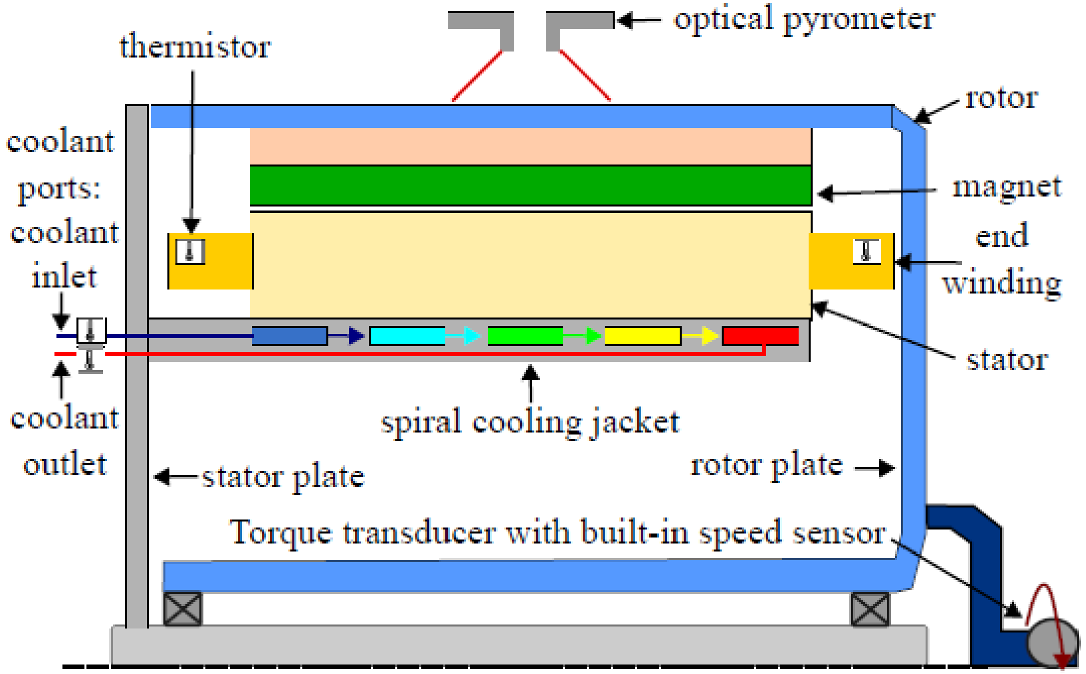

Figure 5. In-wheel motor back-to-back test setup and Cross-section of the machine.

LPTN Identification

Particle Swarm Optimization was used to estimate the LPTN.

100 iterations were used to estimate the LPTN.

Each iteration evaluates a population (Swarm Size) of 220 individuals.

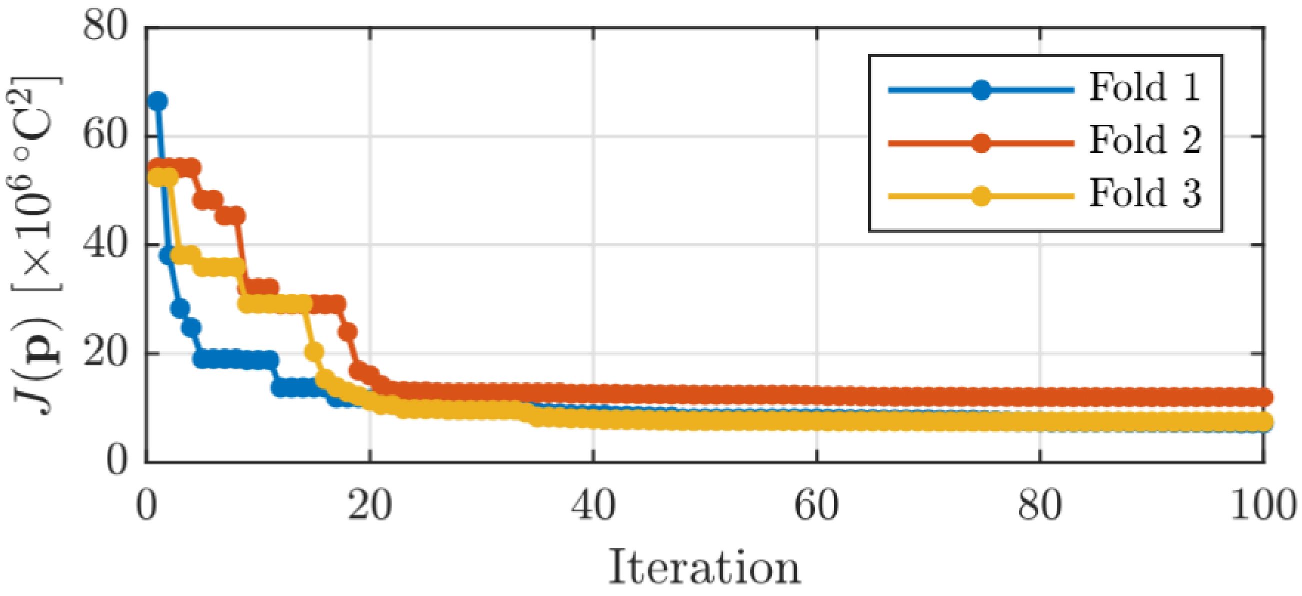

Figure 5. Cost function reduction for the LPTN Estimation process.

Table 1. Identified thermal network parameters per fold.

Parameter	Unit	Fold 1	Fold 2	Fold 3
C_{m}	J/K	6846	6652	6834
C_{t}		1167	3043	3222
C_{w}		5738	5296	5533
C_{y}		1649	3340	2979
$R_{\mathrm{cy},0}$	K/W	0.005	0.004	0.004
$R_{\mathrm{tm},0}$		0.408	0.484	0.402
$R_{\mathrm{wm},0}$		0.682	0.665	0.579
$R_{\mathrm{w,t}}$		0.522	0.436	0.362
$R_{\mathrm{y,t}}$		0.015	0.015	0.016
$R_{\mathrm{y,w}}$		0.009	0.009	0.009
$R_{\mathrm{ma},0}$		0.305	0.314	0.291
a_{tm}		0.078	0.094	0.071
a_{wm}		0.418	0.492	0.499
a_{ma}		0.032	0.036	0.028
b_{ma}	–	0.187	0.176	0.204
b_{tm}		0.356	0.200	0.248
b_{wm}		1.198	0.968	0.804
k_0	–	0.697	0.775	0.800
k_1		−0.085	−0.080	−0.092
k_2		−0.008	−0.008	−0.005
k_3		−0.159	−0.115	−0.165
α_{cy}	1/K	−0.009	−0.009	−0.008

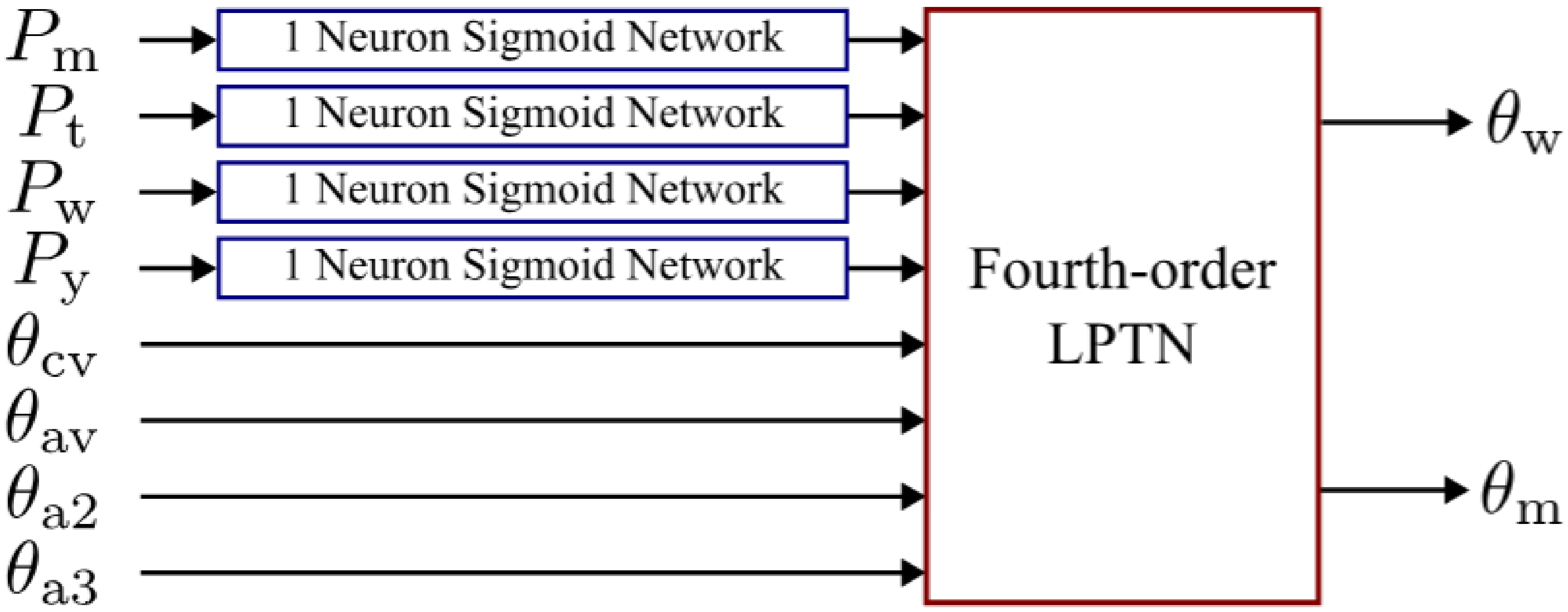

Figure 6. Hammerstein Model Structure.

Estimation considerations:

- Fitted via the Levenberg Marquart algorithm with 100 iterations.
- The zeros of the linear block were assumed to be free parameters.
- The data was normalized.

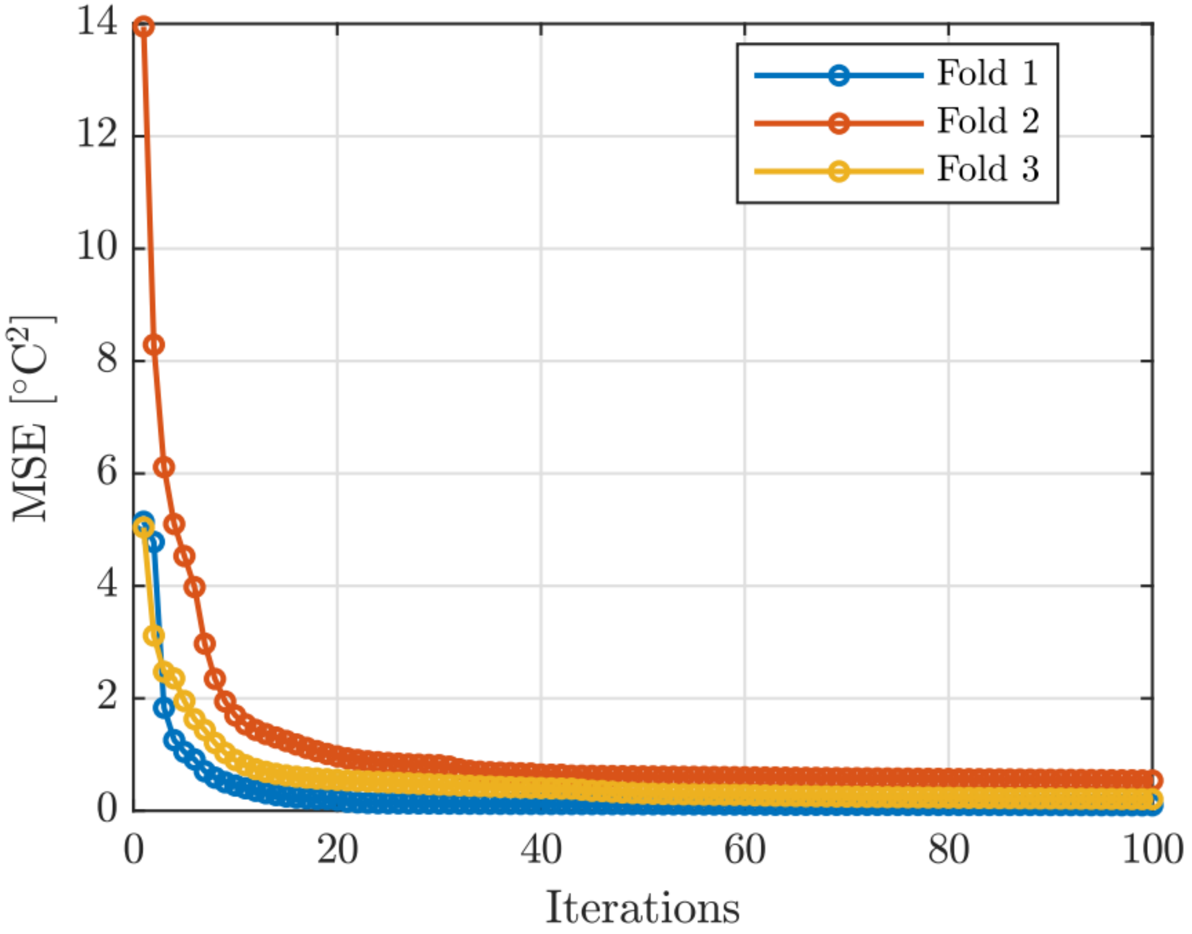

Figure 7. Cost function reduction of the Hammerstein model.

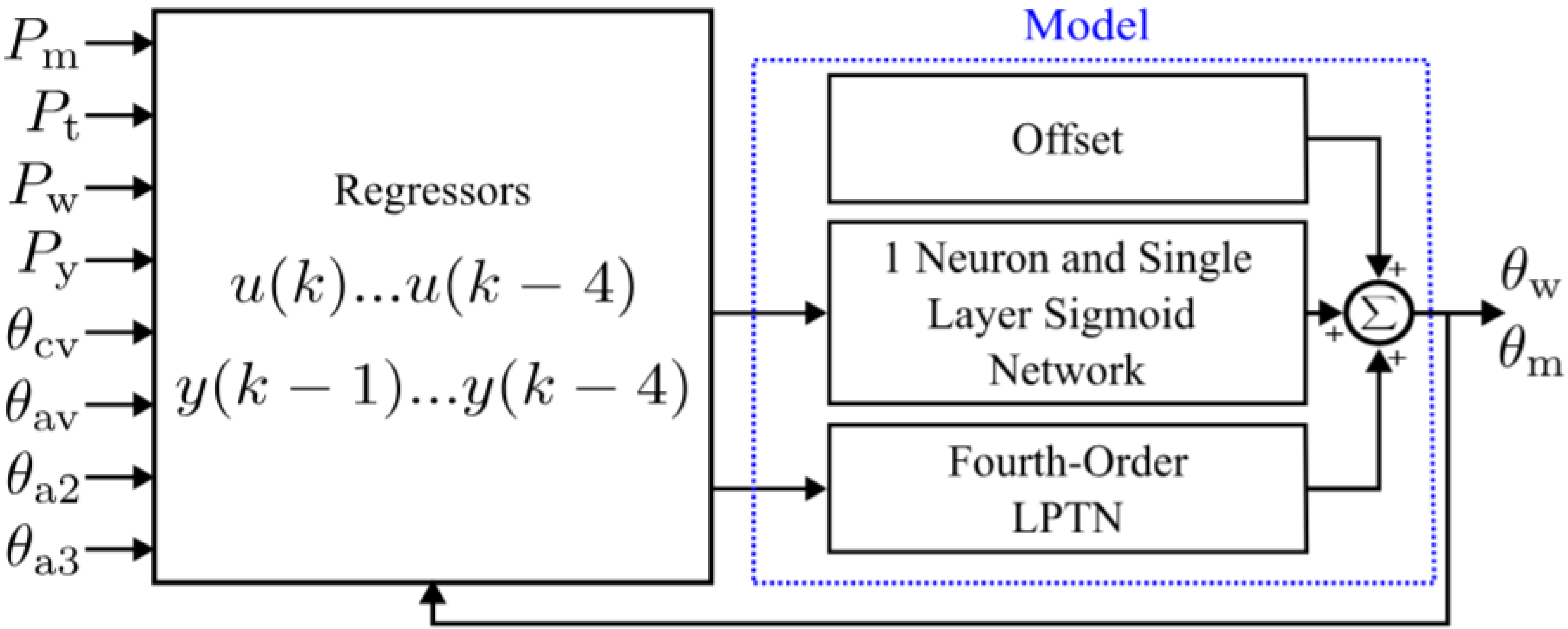

Figure 8. NLARX model structure initialized with the thermal network.

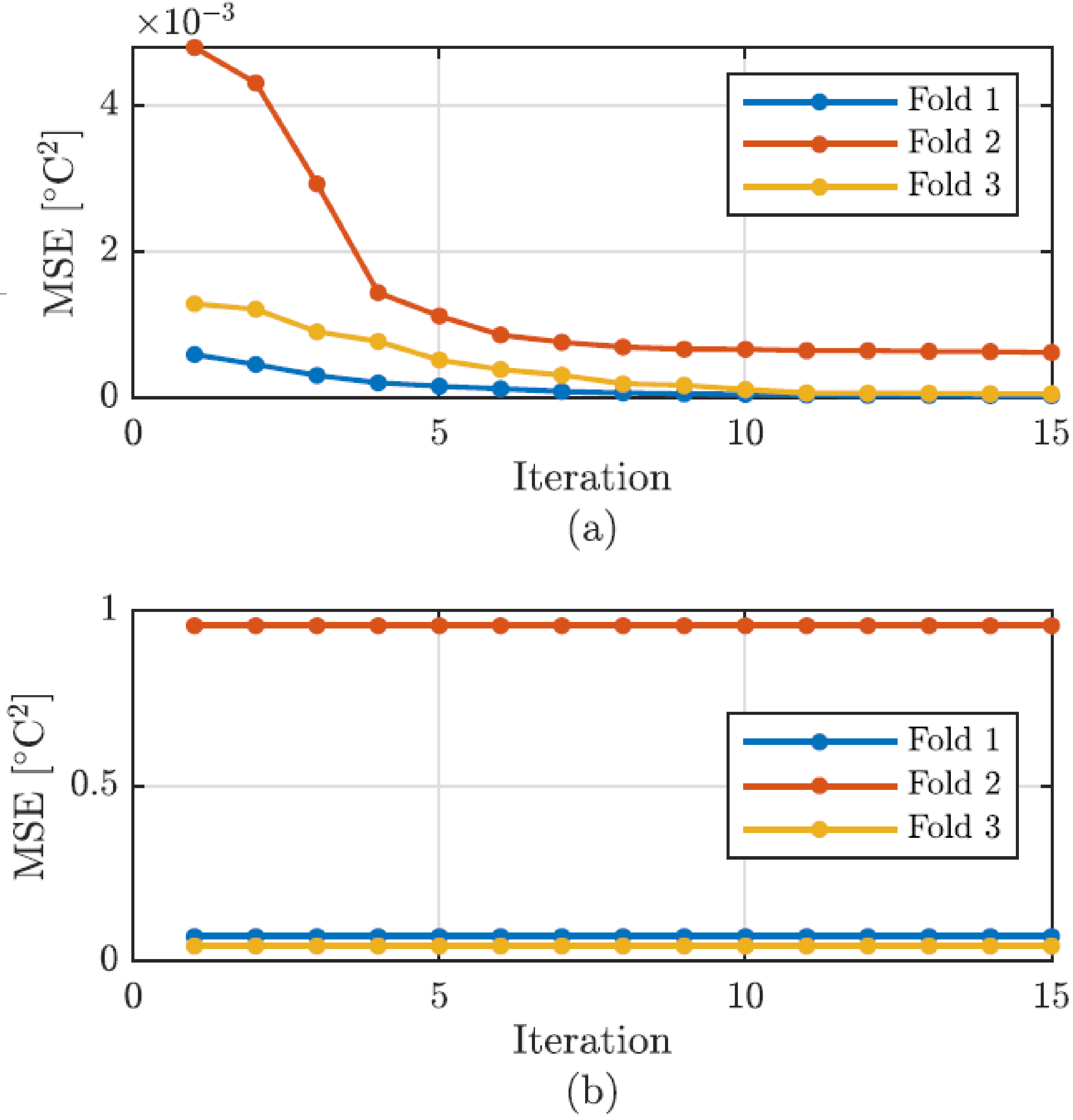

Figure 9. NLARX cost function reduction.

Table 1. Validation performance of the LPTN, Hammerstein Model, and NLARX model.

Metric	LPTN		HM		NLARX	
	Wdg.	PM	Wdg.	PM	Wdg.	PM
Fold 1						
MSE [$^\circ C^2$]	12.78	1.165*	3.953	1.280	3.144*	1.384
RMSE [$^\circ C$]	3.575	1.080*	1.988	1.132	1.773*	1.177
MAE [$^\circ C$]	3.135	0.851*	1.742	0.936	1.554*	1.087
$\|e\|_\infty$ [$^\circ C$]	6.476	2.725	5.871	3.146	3.796*	2.628*
R^2	0.985	0.946*	0.995	0.941	0.996*	0.936
NRMSE	0.123	0.232*	0.069	0.243	0.061*	0.253
Fold 2						
MSE [$^\circ C^2$]	10.28	0.632	1.400*	0.479	3.234	0.396*
RMSE [$^\circ C$]	3.207	0.795	1.183*	0.692	1.798	0.629*
MAE [$^\circ C$]	3.055	0.692	1.015*	0.572	1.548	0.555*
$\|e\|_\infty$ [$^\circ C$]	5.328	1.775	4.513*	2.628	5.887	1.347*
R^2	0.988	0.975	0.998*	0.981	0.996	0.984*
NRMSE	0.111	0.159	0.041*	0.138	0.063	0.126*
Fold 3						
MSE [$^\circ C^2$]	8.669	0.293	0.630	0.330	0.492*	0.081*
RMSE [$^\circ C$]	2.944	0.541	0.793	0.574	0.702*	0.285*
MAE [$^\circ C$]	2.660	0.434	0.592	0.452	0.527*	0.221*
$\|e\|_\infty$ [$^\circ C$]	5.232	1.463	3.410	2.371	2.279*	1.073*
R^2	0.990	0.987	0.999	0.985	0.999*	0.996*
NRMSE	0.102	0.116	0.027	0.123	0.024*	0.061*

*Best performance

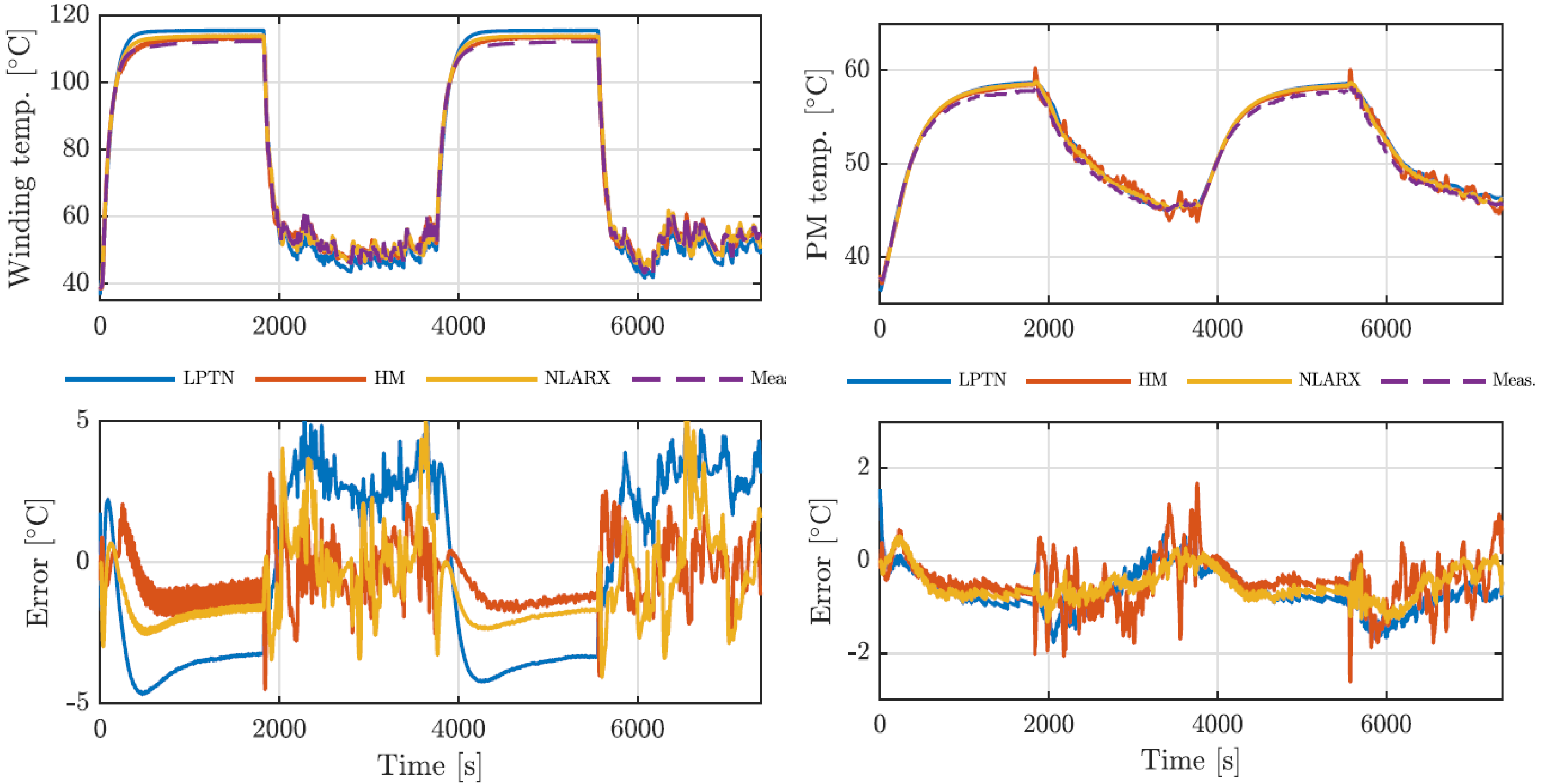

Figure 9. Winding and magnet temperature estimation comparison between the thermal network, Hammerstein model, and NLARX model.

Table 2. Average performance of the LPTN, Hammerstein Model, and NLARX model.

Metric	LPTN				HM				NLARX			
	Winding		PM		Winding		PM		Winding		PM	
	Avg.	Std. dev.	Avg.	Std. dev.	Avg.	Std. dev.	Avg.	Std. dev.	Avg.	Std. dev.	Avg.	Std. dev.
MSE [°C^2]	10.58	2.072	0.697	0.440	1.994*	1.739*	0.696	0.511	2.290	1.558	0.621*	0.680*
RMSE [°C]	3.242	0.317	0.805	0.269	1.322*	0.609*	0.799	0.294	1.424	0.626	0.697	0.450*
MAE [°C]	2.950	0.255	0.659	0.210	1.116*	0.582*	0.653	0.252	1.210	0.591	0.6212*	0.4366*
$\|e\|_\infty$ [°C]	5.679	0.692	1.988	0.657	4.598	1.233	2.715	0.395	3.987*	1.812*	1.683*	0.830*
R^2	0.987	0.003	0.969	0.021	0.998*	0.002*	0.969	0.024	0.997	0.002	0.972*	0.032*
NRMSE	0.112	0.012	0.169	0.059	0.046*	0.021*	0.168	0.065	0.049	0.022	0.147*	0.098*

*Best performance

Table 3. Average training time and execution time comparison of the thermal network, Hammerstein model, and NLARX model.

Model	Parameters	Avg. Training Time [s]	Std. Dev. Training [s]	Execution Time [μs]	CPU Util. [%]
LPTN	22	$46 \cdot 10^3$	209	60.7	0.003
HM	136	23	3.8	161	0.008
NLARX	150	44	42.5	1417	0.071

Training Hardware: AMD Ryzen 9 3950X 16-core processor (3.49GHz) and 64 GB of RAM
Execution Hardware: C2000TM LaunchPad with a TMS320F28069M microcontroller operating at 90 MHz

Conclusions and Future Work

Hammerstein and NLARX models were used to estimate winding and magnet temperatures in a permanent magnet synchronous motor.

Models were initialized using a fourth-order thermal network.

Speed- and temperature-dependent thermal resistances were included as inputs to capture their effects.

- Thermal network estimation error: 10.578 °C² (winding) and 0.697 °C² (magnet).
- Hammerstein model estimation error: 1.994 °C² (winding) and 0.696 °C² (magnet).
- Nonlinear autoregressive model estimation error: 2.290 °C² (winding) and 0.621 °C² (magnet).

Conclusions and Future Work

- The nonlinear autoregressive model provided a slight improvement in magnet temperature estimation, whereas the Hammerstein model performed significantly better for winding temperature estimation.

- Future work includes testing different-order thermal networks with both models, applying them to other motors and conditions, and evaluating the feasibility of real-time implementation.

References

1. J. -G. Lee and D. -K. Lim, "A Stepwise Optimal Design Applied to an Interior Permanent Magnet Synchronous Motor for Electric Vehicle Traction Applications," in IEEE Access, vol. 9, pp. 115090-115099, 2021.
2. Z. Wang, J. Chen, M. Cheng and K. T. Chau, "Field-Oriented Control and Direct Torque Control for Paralleled VSIs Fed PMSM Drives With Variable Switching Frequencies," in IEEE Transactions on Power Electronics, vol. 31, no. 3, pp. 2417-2428, March 2016.
3. D. -K. Hong, W. Hwang, J. -Y. Lee and B. -C. Woo, "Design, Analysis, and Experimental Validation of a Permanent Magnet Synchronous Motor for Articulated Robot Applications," in IEEE Transactions on Magnetics, vol. 54, no. 3, pp. 1-4, March 2018.
4. T. Orlowska-Kowalska et al., "Fault Diagnosis and Fault-Tolerant Control of PMSM Drives–State of the Art and Future Challenges," in IEEE Access, vol. 10, pp. 59979-60024, 2022.
5. M. Ehsani, Y. Gao and J. M. Miller, "Hybrid Electric Vehicles: Architecture and Motor Drives," in Proceedings of the IEEE, vol. 95, no. 4, pp. 719-728, April 2007.
6. O. Wallscheid, "Thermal Monitoring of Electric Motors: State-of-the-Art Review and Future Challenges," in IEEE Open Journal of Industry Applications, vol. 2, pp. 204-223, 2021.
7. He, L., Feng, Y., Zhang, Y. et al. Methods for temperature estimation and monitoring of permanent magnet: a technology review and future trends. J Braz. Soc. Mech. Sci. Eng. 46, 174 (2024).
8. Schoukens, M., & Tiels, K. (2017). Identification of block-oriented nonlinear systems starting from linear approximations: A survey. Automatica, 85, 272-292.
9. O. Wallscheid and J. Böcker, "Global Identification of a Low-Order Lumped-Parameter Thermal Network for Permanent Magnet Synchronous Motors," in IEEE Transactions on Energy Conversion, vol. 31, no. 1, pp. 354-365, March 2016.

Hardware Implementation Considerations of the Hammerstein Model

32-BIT HARDWARE IMPLEMENTATION

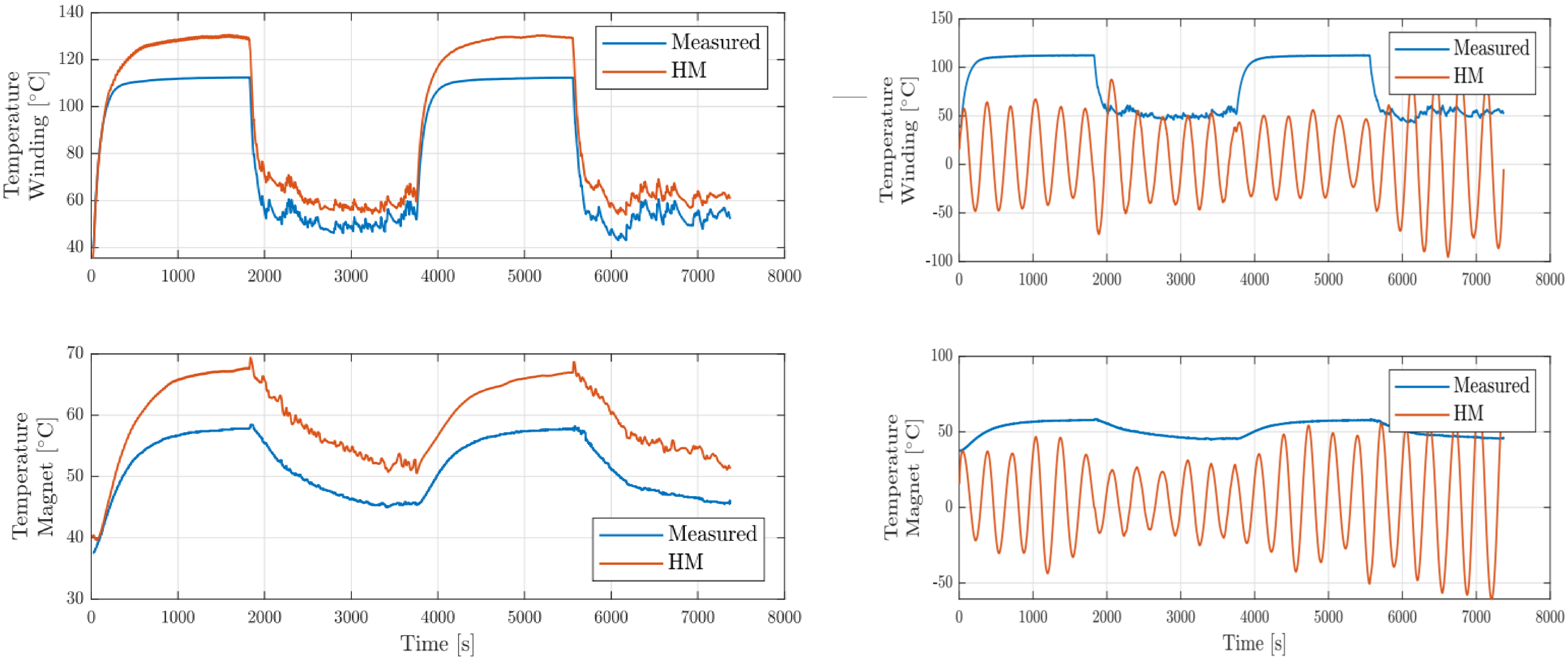

Dynamics of the Hammerstein model model alterated by truncating its parameters from double to Single precision

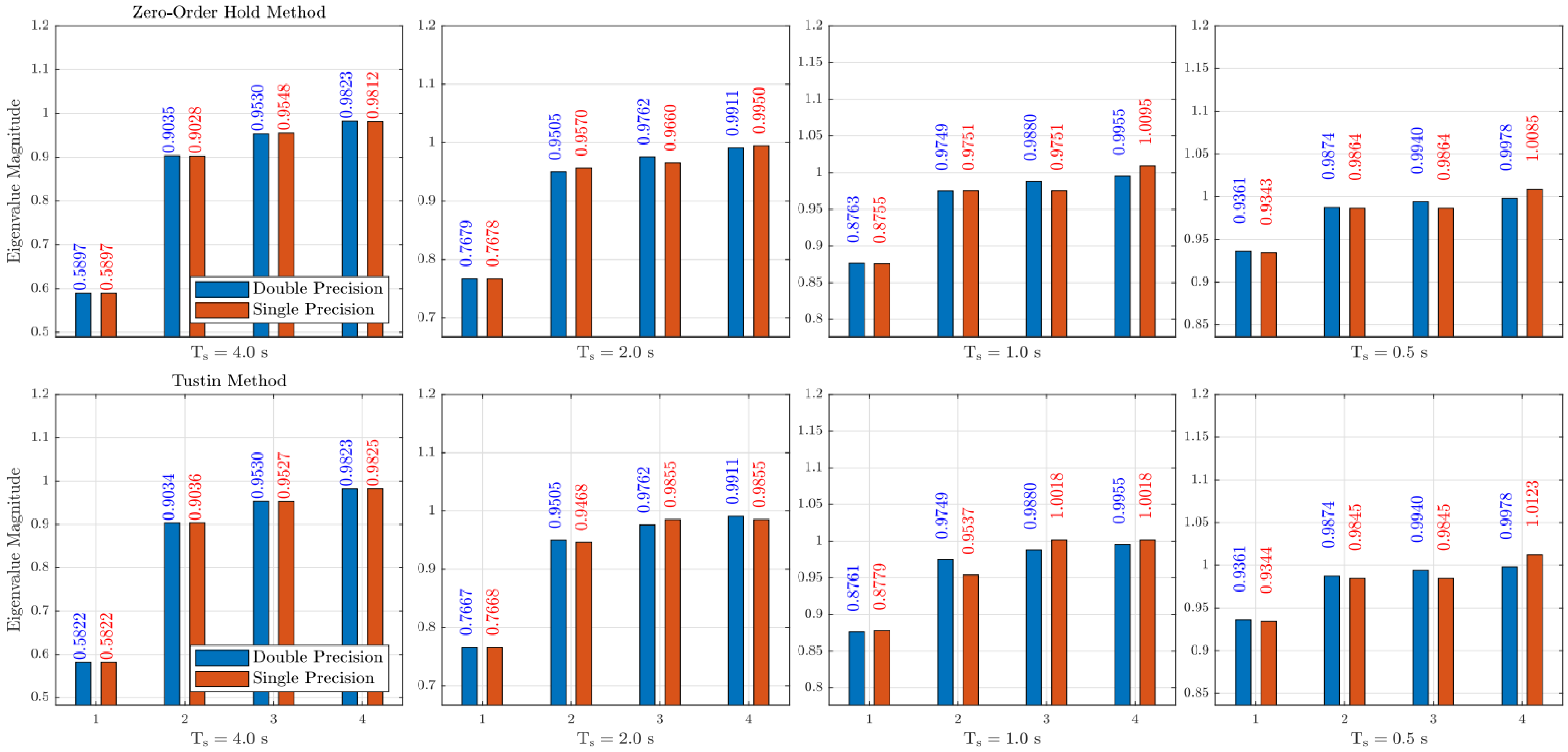

Eigenvalue comparison of the state-transition matrix of the Hammerstein Model linear block between double and single precision.

Ill-Conditioned Model

Linear Block
in
State-Space Form

→

For estimating the model the linear block its converted from state space form to polynomial form

→

After estimating the model the polynomial form of the linear bock is converted back to state space form but in companion form

The change in model dynamics when translating the Hammerstein model from double to single precision is due to the ill-conditioning of the linear component’s state-transition matrix.

This matrix’s high sensitivity to eigenvalues arises because the Hammerstein model is initially expressed in an inherently ill-conditioned polynomial form.

When converted to state-space form, it takes on an ill-conditioning companion form.

$$\kappa(A) = \|A\| \cdot \|A^{-1}\|$$

A condition number close to one indicates a well-conditioned matrix, while a higher condition number signifies an ill-conditioned matrix

The condition number of the state-transition matrix was computed to analyzed the numerical stability.

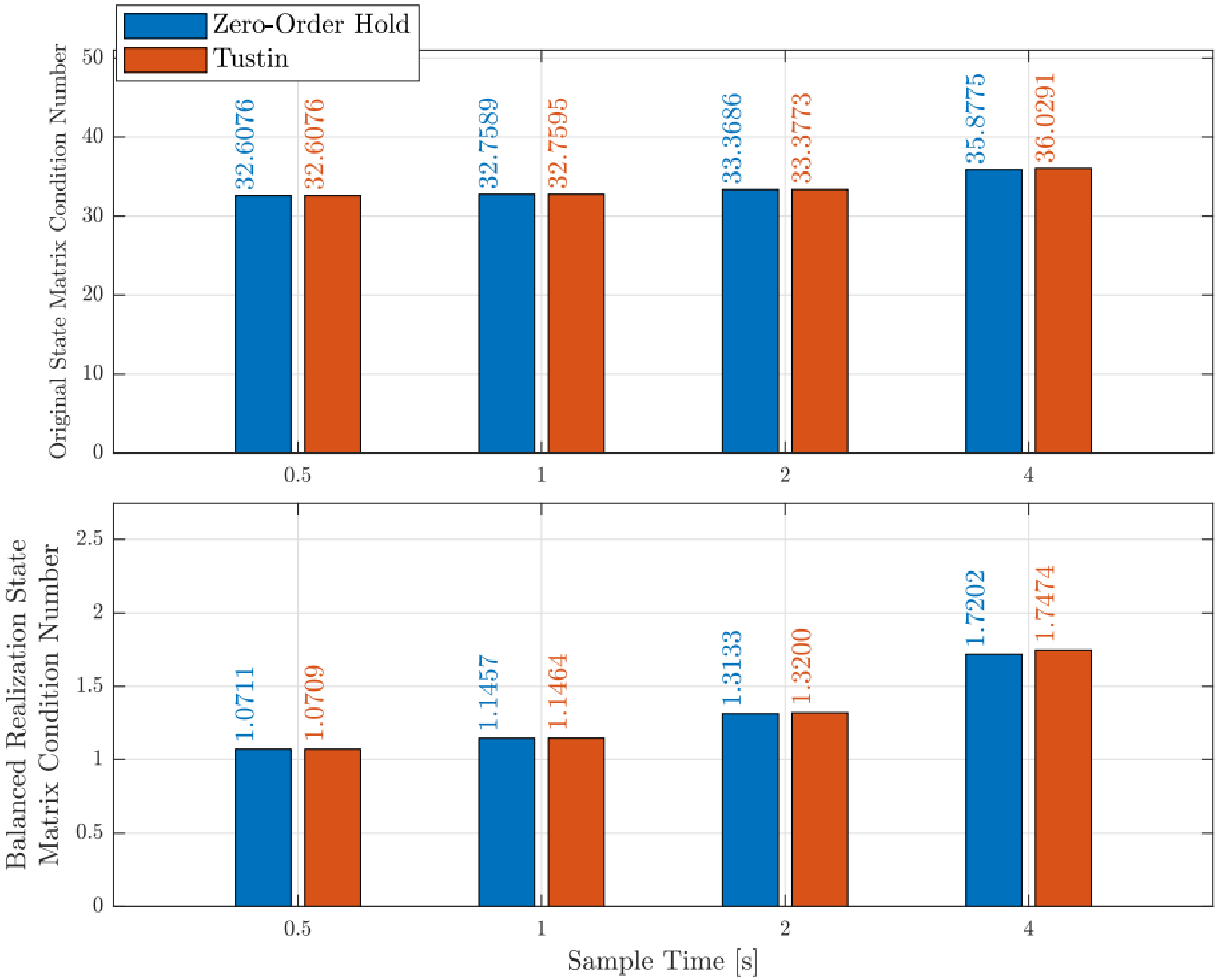

Condition Number of the state-transition matrix between the original model and balanced realization.

Balanced State Space Realization

$$\dot{x}(t) = Ax(t) + Bu(t),$$
$$y(t) = Cx(t) + Du(t)$$

Definition: A balancing transformation is a coordinate transformation that makes system states equally controllable and observable.

$$AW_c + W_cA^T + BB^T = 0,$$
$$A^TW_o + W_oA + C^TC = 0.$$

$$\hat{W}_c = \hat{W}_o = \Sigma \qquad W_cW_oT = T\Sigma^2$$

Uses: Improves numerical stability and reduces system order in model reduction.

$$T_s = T\Sigma_s \qquad \Sigma_s = \Sigma_c^{1/4}\Sigma_o^{-1/4}$$

$$A_{\mathrm{bal}} = T_s^{-1}AT_s, \quad B_{\mathrm{bal}} = T_s^{-1}B, \quad C_{\mathrm{bal}} = CT_s.$$

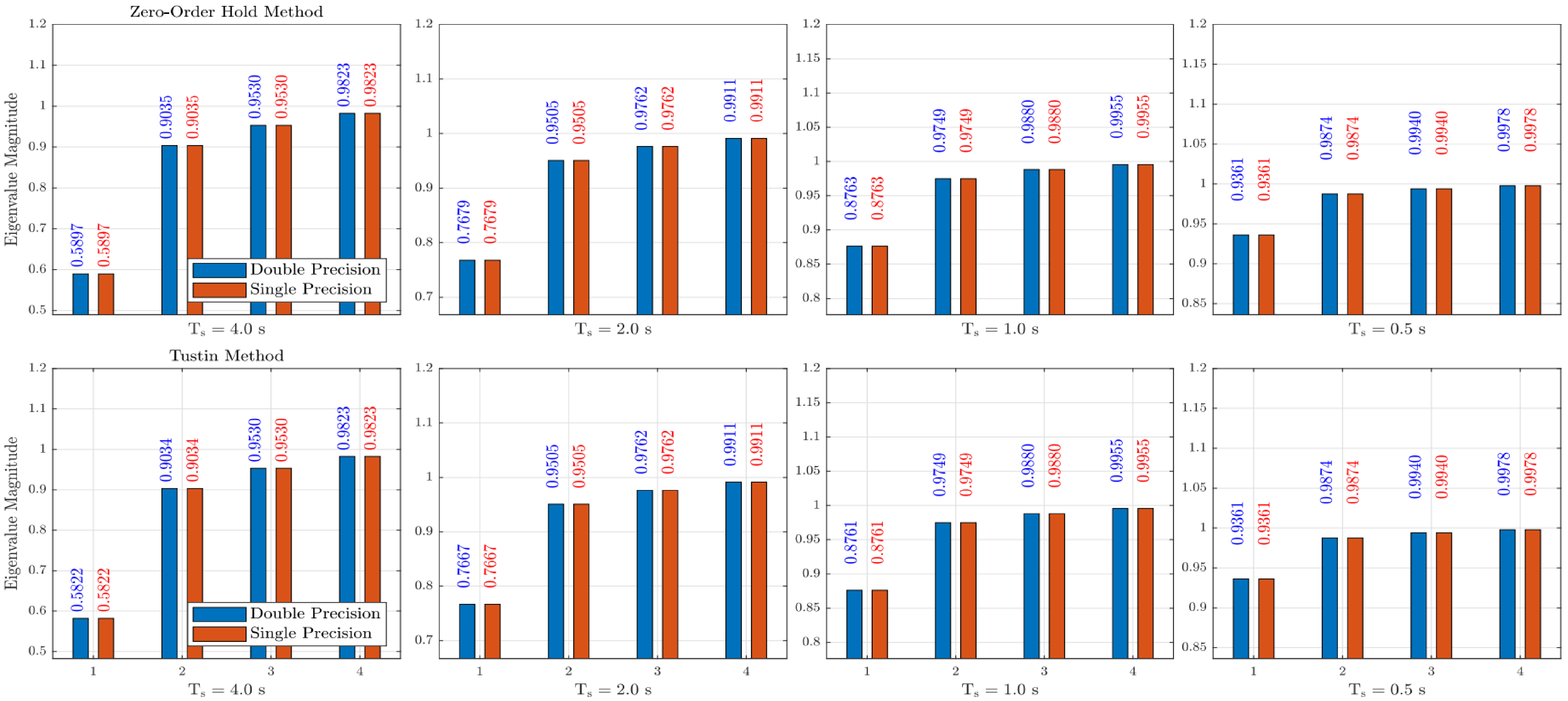

Eigenvalue comparison of the balanced realization of the state-transition matrix of the Hammerstein Model linear block between double and single precision.

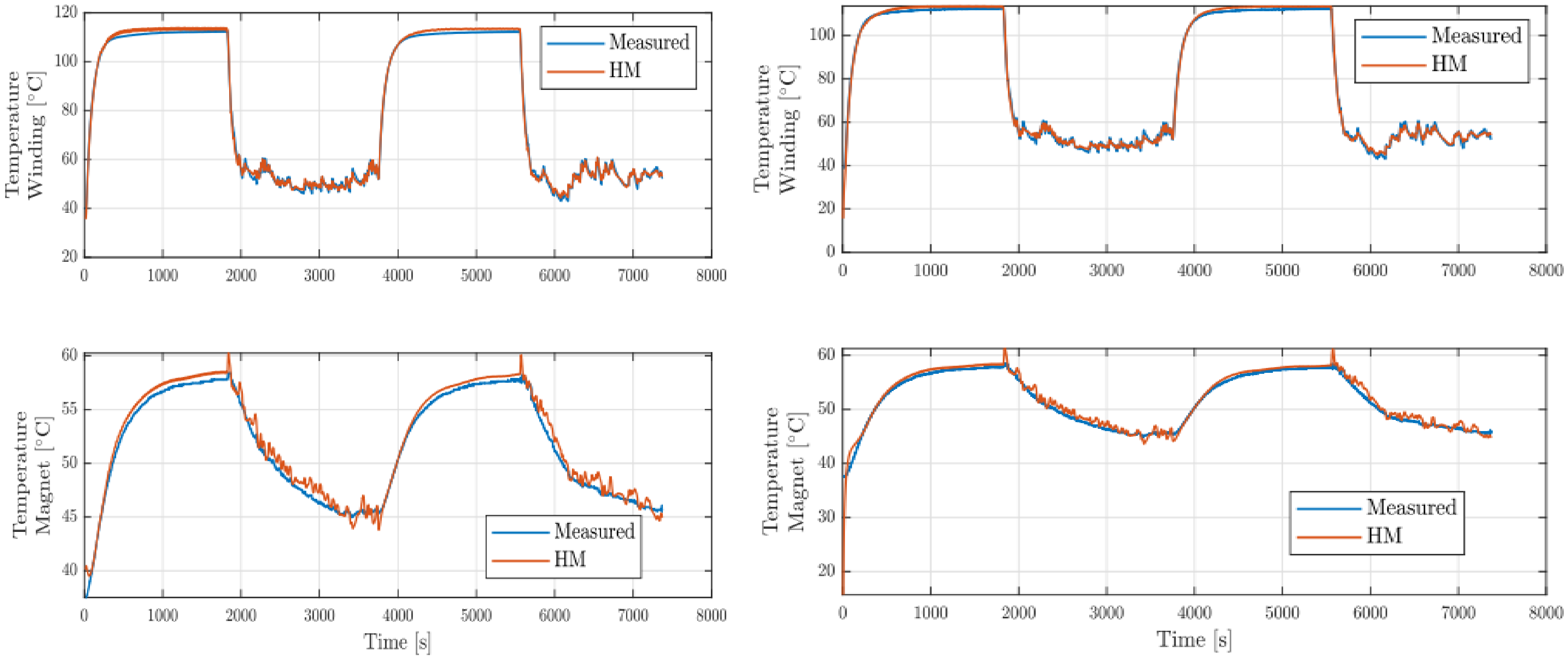

Dynamics of the Hammerstein model by balancing the linear block of the Hammerstein model.

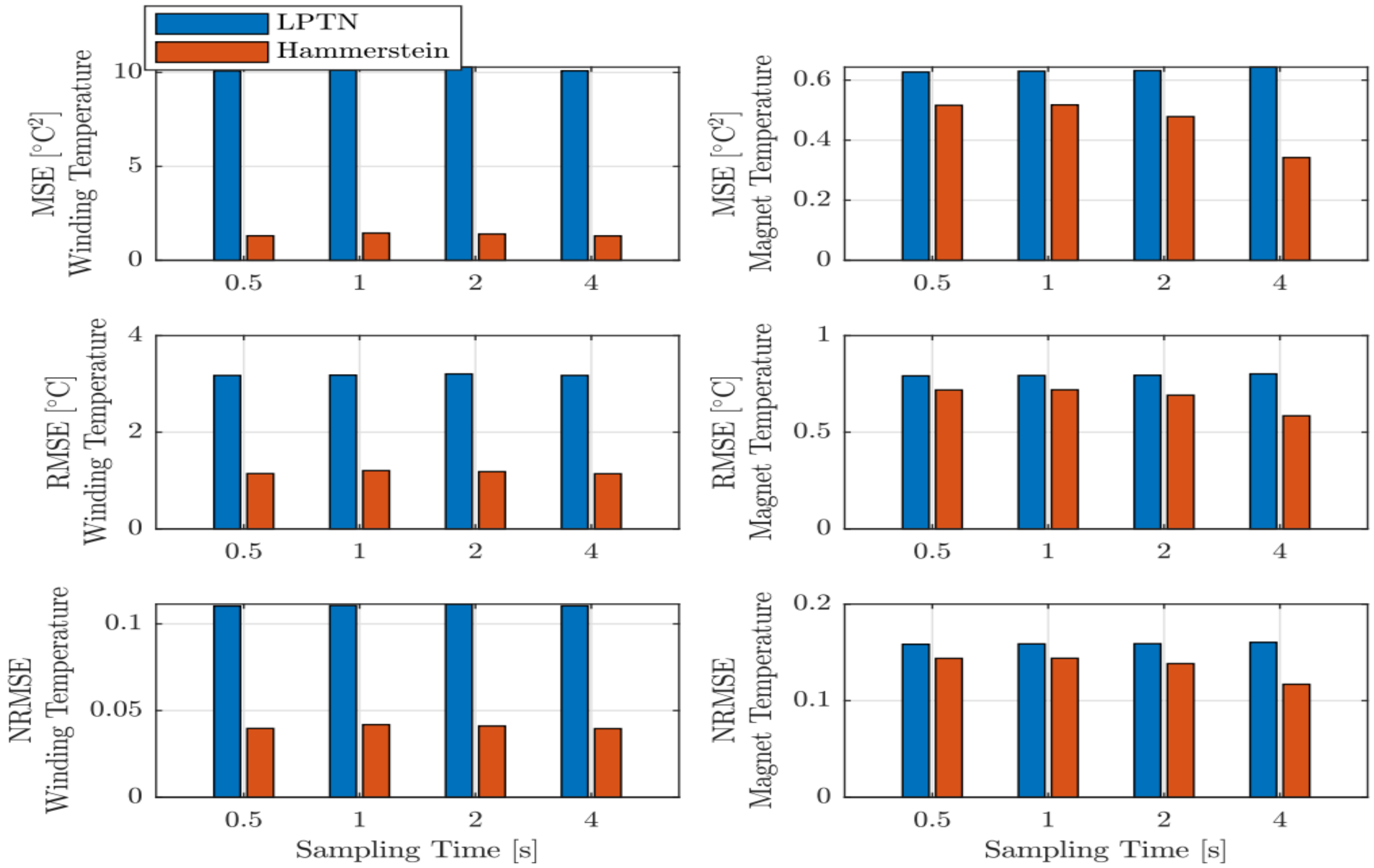

Performance of the temperature estimation for the winding and magnet of the Hammerstein and LPTN models for different sampling rates. The left plots show the winding temperature estimation errors. The right plots show the magnet temperature estimation errors.

Processor in the Loop Simulation

The model is executed in the actual target processor.

C2000TM LaunchPadXL **TMS320F28069M**. 90 MHz clock and single precision floating point unit.

Measure Average Execution Time, Initialization Time, and Termination Time.

$$CPU\ Utilization = \frac{Execution\ Time}{Sampling\ Time} 100\%$$

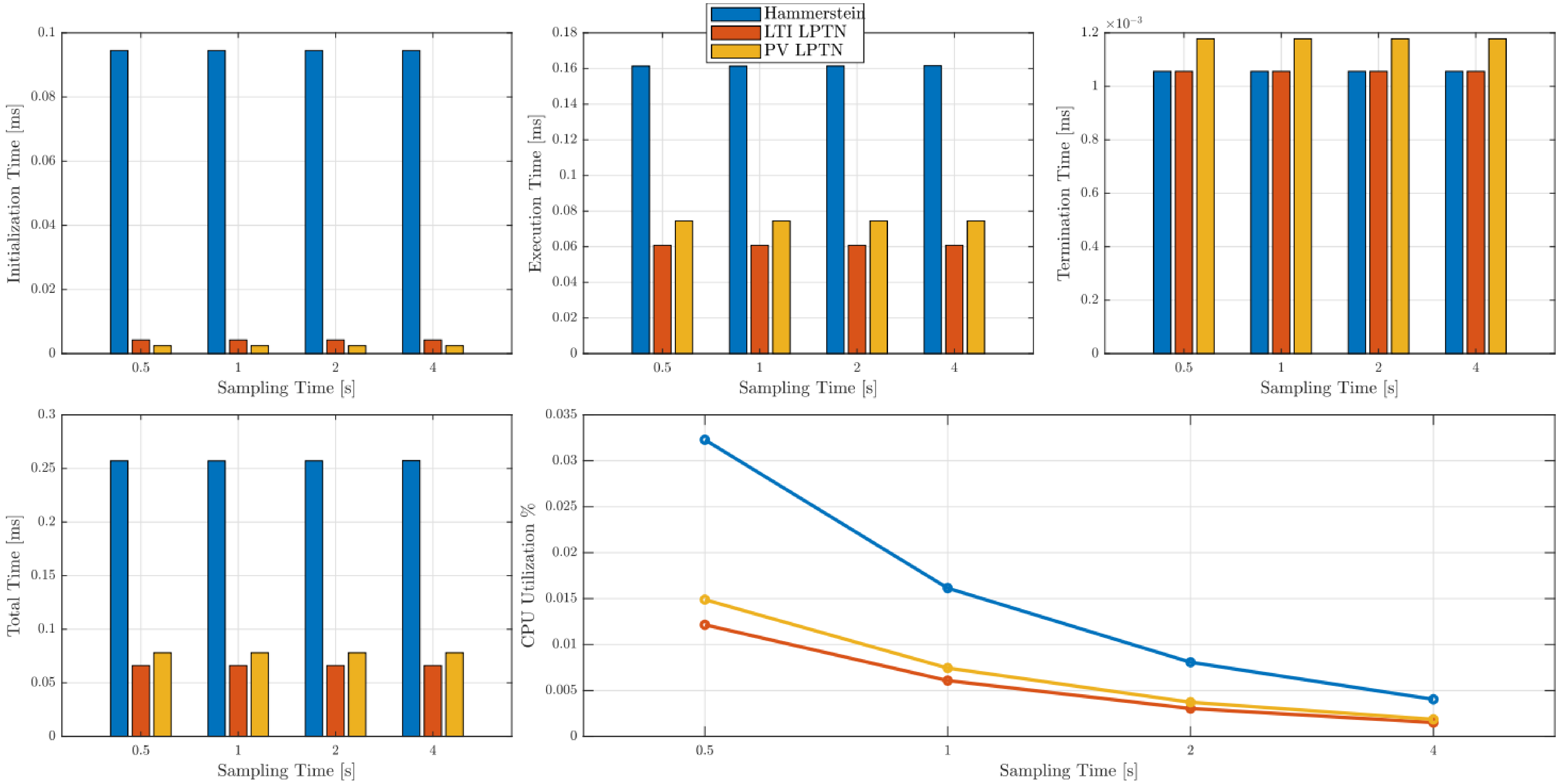

Comparison of Execution Time of the Hammerstein model with the LPTN.